2018 7th IEEE International Conference on Biomedical
Robotics and Biomechatronics (Biorob)
Enschede, The Netherlands, August 26-29, 2018

Improving the Standing Balance of Paraplegics through the use of a Wearable Exoskeleton*

Amber Emmens[1], Edwin van Asseldonk[1], Marcella Masciullo[2], Matteo Arquilla[2], Iolanda Pisotta[2], Nevio Luigi Tagliamonte[2], Federica Tamburella[2], Marco Molinari[2] and Herman van der Kooij[1,3]

Abstract— **In this study, our goal was to improve the standing balance of people with a spinal cord injury by using a wearable exoskeleton that has ankle and knee actuation in the sagittal plane.**

Three test-pilots that have an incomplete spinal cord injury wore the exoskeleton and tried to maintain standing balance without stepping while receiving anteroposterior pushes. Two balance controllers were tested: one providing assistance based on the subject's body sway and one based on the whole body momentum. For both controllers, the balance performances of the test-pilots wearing the exoskeleton were assessed based on the center of mass kinematics and compared to the condition in which the device did not provide any assistance.

One of the test-pilots was not able to maintain balance without assistance, but could withstand small pushes when any of the balance controllers was implemented. For this test-pilot the recovery time and sway amplitude hardly varied with the type of balance controller that was used. For the other two test-pilots the recovery time and the sway amplitude were smallest using the body sway controller.

In conclusion, the wearable exoskeleton with balance controller was able to improve the balance performance of the test-pilots by reducing the recovery time after a perturbation and by enabling one of the test-pilots to maintain balance, who could not maintain balance by himself.

I. INTRODUCTION

Many exoskeletons have been designed to provide support to people with a neurological disorder, such as a spinal cord injury (SCI). Their aims are to help paraplegics to recover [1], [2], [3], [4], [5] or to restore gait in daily life [6], [7], [8]. Research on exoskeletons for people that have a SCI mainly focusses on walking, although balance is generally also affected. Wearable exoskeletons rely on crutches for balance maintenance [7], [3], [9], which prevents users from using their arms for other activities of daily living. Although balance is an important issue in exoskeleton control, only a few studies have addressed the topic of exoskeleton balance control during walking [10], [6] or standing [11], [12].

In human standing balance center of mass (CoM) motion plays an important role. Therefore, in a previous study, a balance control strategy based on the CoM-related body sway was designed and tested on healthy subjects wearing a powered ankle-foot orthosis [12]. The ankle torques that the orthosis should deliver followed directly from a proportional-derivative (PD) control law that used the body sway angle and velocity as an input. It was shown that this controller could provide effective, human-like supportive torques, but results were not directly generalizable to people with a SCI.

In the field of humanoid robotics momentum-based control strategies have been applied to impose balancing on a robot [13], [14], [15]. These controllers aim to regulate the linear and angular component of the whole body momentum. Since the derivative of the whole body momentum is related to generalized accelerations [16], one can define an optimization routine to find generalized accelerations such that this derivative is as close as possible to a certain desired value [14], [15]. Given the successful implementations of momentum-based controllers in humanoid experiments, paraplegics using a wearable exoskeleton may also benefit from this type of balance control.

Our goal is to improve the balance of people with a SCI through the use of a wearable exoskeleton. Therefore, as a case study, we implemented a body sway controller and momentum-based controller on a wearable exoskeleton that has ankle and knee actuation and evaluated whether these controllers can improve the standing balance recovery in the sagittal plane of three test-pilots that have a SCI.

II. METHODS

A. Test-Pilots

Three male test-pilots that have a SCI participated in the balance experiments. Their characteristics are shown in table I. Ethical approval for the experimental protocol was given by the Ethical Committee of Fondazione Santa Lucia, Italy (Prot. CE/PROG. 509).

B. Wearable Exoskeleton

Fig. 1 shows an overview of the Wearable Exoskeleton (WE) that was used in the experiments. It consists of separate ankle and knee modules, which can be connected through toggle latches, and a backpack. The WE has four series-elastic actuators that can provide flexion/extension torques to the knees and plantar/dorsiflexion torques to the ankles, while the ankle inversion/eversion is left free. The rotations of the ankle and knee joints are measured with encoders. A detailed description of the device is presented in the work of Meijneke et al. (2016) [17].

*SYMBITRON is supported by EU research program FP7-ICT-2013-10 (contract #611626). SYMBITRON is coordinated by University of Twente.

[1]Amber Emmens, Edwin van Asseldonk and Herman van der Kooij are with the Biomechanical Engineering Department, University of Twente, 7500 AE Enschede, The Netherlands a.r.emmens@utwente.nl

[2]Marcella Masciullo, Matteo Arquilla, Iolanda Pisotta, Nevio Tagliamonte, Federica Tamburella and Marco Molinari are with the Laboratory of Robotic Neurorehabilitation, Fondazione Santa Lucia, Rome, Italy

[3]Herman van der Kooij is with the Biomechanical Engineering Department, Delft University of Technology, Delft, The Netherlands

978-1-5386-8183-1/18/$31.00 ©2018 IEEE

TABLE I

TEST-PILOT CHARACTERISTICS, TRIAL ORDER, CONTROLLER SETTINGS AND MAXIMUM PUSH IMPULSE.

	Info			Trial Order	Controller settings									Max Push (Ns)
	height (m)	mass (kg)	lesion level		K_{pA} ($\frac{Nm}{rad}$)	K_{dA} ($\frac{Nms}{rad}$)	K_{pK} ($\frac{Nm}{rad}$)	K_{dK} ($\frac{Nms}{rad}$)	Γ_K ($\frac{1}{s}$)	Γ_{Lx} ($\frac{1}{s}$)	Γ_{Rx} ($\frac{1}{s^2}$)	FF_A (N)	FF_K (N)	
TP1	1.65	80	C7	PD_{com}, MBC, ZI	280	53.4	35.0	7.00	1.66	0.166	3.30	0	0	30
TP2	1.70	80	L4-S3	PD_{com}, ZI, MBC*	774	89.2	141	28.1	1.65	0.099	3.28	10	-10	10
TP3	1.73	76	T10-T11	ZI, PD_{com}, MBC	479	70.0	34.2	6.84	1.64	0.164	3.21	0	0	30

* Collected on a different day

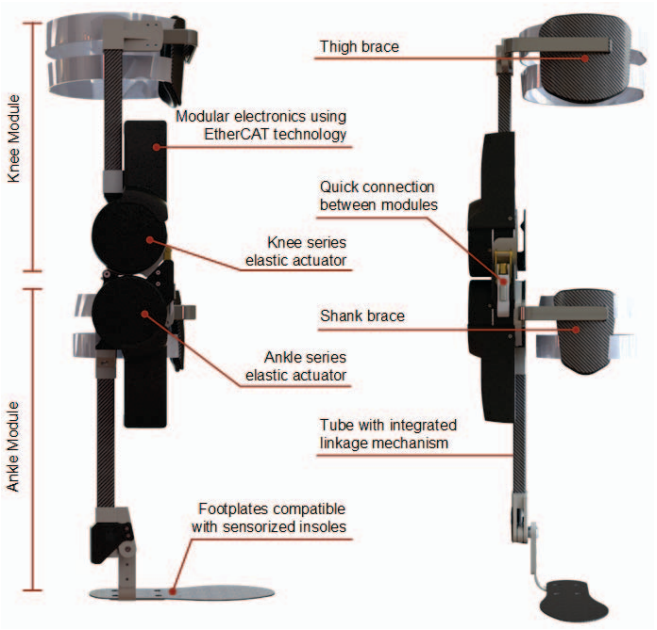

Fig. 1. Overview of the wearable exoskeleton that was used in the experiments.

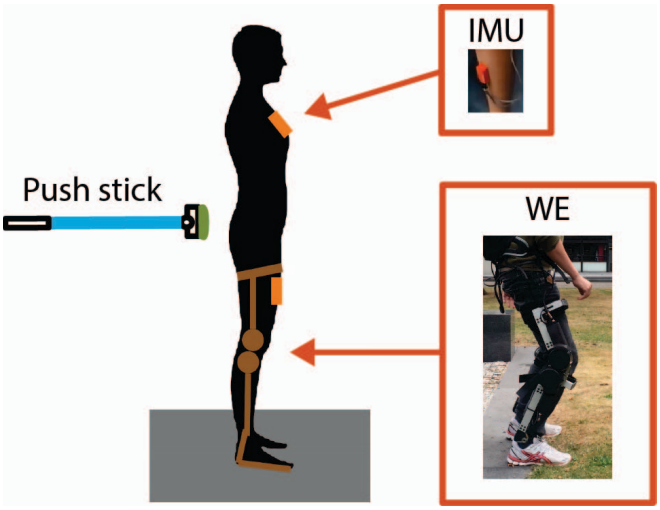

Fig. 2. Overview of the experimental setup.

To get a modular design for real-time control, the exoskeleton is controlled using EtherCAT. The backpack contains a computer (EtherCAT Master) that communicates with custom-made EtherCAT slave electronics in the actuation units, such as a motor controller. During the experiments subjects did not wear the backpack, but it was placed behind them on a chair. An overview of the experimental setup is shown in Fig. 2.

C. Control Strategies

1) Body Sway Control: In the body sway control strategy, PD_{com}, the knee and ankle joints are controlled independently. The ankle controller computes desired ankle torques based on the body sway, while the knee controller tries to keep the knee stretched. The desired ankle torque τ_{A_d} is derived from a PD-control law:

$$\tau_{A_d} = K_{pA}(\theta_{sway_d} - \theta_{sway}) + K_{dA}(\dot{\theta}_{sway_d} - \dot{\theta}_{sway}) \quad (1)$$

where K_{pA} and K_{dA} are proportional and derivative gains respectively, θ_{sway} is the body sway angle that is dependent on the CoM location (Fig. 3C), and subscript d indicates a desired value. Note that the desired ankle torque is the same for both left and right. To prevent the controller from generating large ankle torques that would make a test-pilot topple over, the desired ankle torque was limited by the forefoot length and the static normal force.

$$\tau_{A_d} \leq Mgl_{ff} \quad (2)$$

Where M is the total mass, g the gravitational acceleration and l_{ff} the forefoot length.

The desired knee torque τ_{K_d} is dependent on the knee angle of the corresponding leg.

$$\tau_{K_d} = K_{pK}(\phi_{K_d} - \phi_K) + K_{dK}(\dot{\phi}_{K_d} - \dot{\phi}_K) \quad (3)$$

where K_{pK} and K_{dK} are proportional and derivative gains respectively and ϕ_K the knee angle.

For each test-pilot proper controller settings were acquired in a separate tuning session. During this session the pilots tested various subsets of controller gains while receiving forward pushes on the trunk with increasing push magnitude. After testing a subset of gains they had to rate the controller based on the perceived safety (S), comfort (C) and assistance (A) from the WE. Together with a performance (P) score, based on the push magnitude that test-pilots could handle without losing balance, a performance and usability index (PUI) was defined:

$$PUI = 0.30S + 0.27C + 0.20P + 0.23A \quad (4)$$

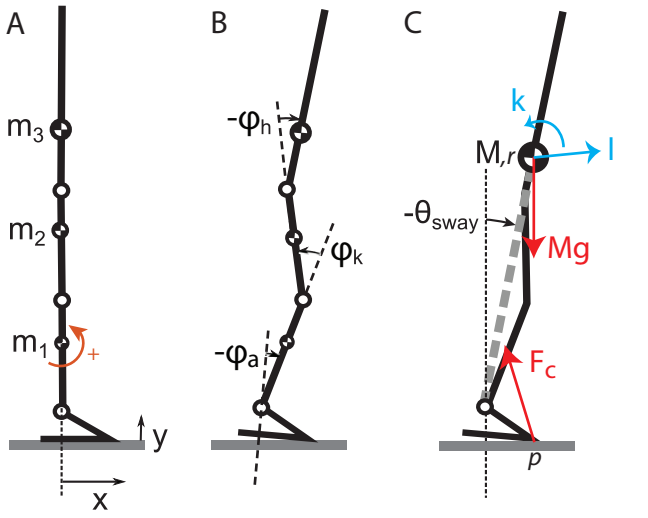

Fig. 3. Computation of controller properties based on a rigid link model. The variables m_n are segment masses, ϕ are the joint angles, θ_{sway} the body sway angle, M the total body mass, k the angular momentum and l the linear momentum. The gravitational force Mg and the ground contact force F_c are applied at the CoM r and center of pressure p respectively. A: model in baseline pose. The model is placed in a right-handed coordinate system. Segment rotations and moments are positive in counter-clockwise direction. B: the joint angles are defined as the angle of segment n minus the angle of segment $n-1$. Segment angles are zero in the baseline pose. C: Forces acting on the model, resulting in a whole body momentum. Based on segment angles and masses the whole body CoM can be computed. Similar to the segment angles, the body sway angle is positive in counter-clockwise direction.

The weights in 4 were defined based on importance ratings given by 3 physical therapists, 3 medical doctors and 4 people with a SCI. The combination of controller gains that resulted in the highest PUI was used in the experiment. The controller gains for each test-pilot are shown in Table I. When test-pilots had difficulties to maintain balance while standing still without receiving pushes, we provided them with a positive or negative feed forward support torque at the ankle or knee respectively such that the test-pilot could stand comfortably. The feed forward ankle torque FF_A and knee torque FF_K for each test-pilot are also shown in Table I.

2) Momentum-based Control: The momentum-based control strategy, *MBC*, tries to find joint torques that generate a certain desired whole-body momentum. The whole-body momentum vector h is composed of the angular momentum about the CoM k and the linear momentum l (Fig. 3C). Since we are only considering the sagittal plane motion, h is a 3×1 vector. It was shown that the whole-body momentum can be expressed as a function of the joint velocities $\dot{\phi}$ through centroidal momentum matrix A_G [16].

$$h = A_G\dot{\phi} \tag{5}$$

Therefore, the momentum rate change $\dot{h}$ is related to the joint accelerations $\ddot{\phi}$, which in turn are related to the joint torques through inverse dynamics. The momentum rate change is also related to the contact wrench λ through the equations of motion (Fig. 3C):

$$\dot{h} = A_G\ddot{\phi} + \dot{A_G}\dot{\phi} = \begin{bmatrix}1 & r_y & -r_x\\ 0 & 1 & 0\\ 0 & 0 & 1\end{bmatrix}\lambda + \begin{bmatrix}0\\0\\-Mg\end{bmatrix} \tag{6}$$

$$\lambda = \begin{bmatrix}p_x f_{cy} - p_y f_{cx}\\ f_{cx}\\ f_{cy}\end{bmatrix} \tag{7}$$

Where r is the CoM, M the total mass, g the gravitational acceleration, p the center of pressure, and f_c the contact forces. Subscripts x and y represent the directions along the anteroposterior axis and longitudinal axis respectively, as shown in Fig. 3A. Through optimization we can then find desired joint accelerations that result in a momentum rate change that is as close as possible to a certain desired value, while satisfying (6) [15]. This desired momentum rate change was derived from the whole-body momentum in a PD-like way [14].

$$\dot{h_d} = \begin{bmatrix}\dot{k_d}\\ \dot{l_d}\end{bmatrix} = \begin{bmatrix}\Gamma_k(k_d - k)\\ \Gamma_l(l_d - l) + \Gamma_r M(r_d - r)\end{bmatrix} \tag{8}$$

Where Γ represent the control gains. The objective function for the optimization problem becomes:

$$f = \| \begin{bmatrix}A_G & 0_{3\times3}\\ W & 0_{3\times3}\end{bmatrix}\begin{bmatrix}\ddot{\phi}\\ \lambda\end{bmatrix} + \begin{bmatrix}-\dot{h}_d + \dot{A}_G\dot{\phi}\\ -W\ddot{\phi}_{ref}\end{bmatrix} \|^2 \tag{9}$$

Where $\dot{h}_d$ is the desired momentum rate change, $\ddot{\phi}_{ref}$ reference joint accelerations that are added to the function to ensure that a solution for the optimization problem can be found [14], [15], and W the weights on these accelerations. Constraints were added to the objective function to prevent torques and joint angles from exceeding their limits, to prevent foot slipping and to enforce the center of pressure to be within the base of support.

Finally, inverse dynamics were applied to find joint torques based on the desired joint accelerations.

Since the WE only has ankle and knee joints, we implemented the computed ankle and knee torques and discarded the computed hip torque. Controller settings were acquired in the same way as for the body sway controller. For the linear momentum and the CoM, we decided to only control the component in x-direction by setting the gains in y-direction to zero, since pushes are applied in the anteroposterior direction. The controller gains for each test-pilot are shown in Table I.

3) Computation of Controller Inputs: The CoM, body sway angle, angular momentum and linear momentum were estimated using a human model with four rigid segments: a foot, shank, thigh and head-arms-trunk segment (Fig. 3). It was assumed that the left and right leg moved symmetrically. Foot, shank and thigh lengths were measured; the length of the head-arms-trunk segment and the segments' inertias, masses and CoM were estimated based on the method described by Winter (2009) [18]. The orientation of the segments is obtained using the joint encoders on the ankles and knees and two Xsens (Xsens Technologies B.V., Enschede, the Netherlands) MTx Inertial Measurement Units (IMUs)

operating at 100 Hz on the right thigh and trunk (Fig. 2). The signals of the IMUs were made available real-time on the EtherCAT Master through a RS232-EtherCAT converter box. The segment angles were expressed with respect to the baseline pose. For this baseline pose, subjects were requested to stand comfortably upright. Then all segment angles and the body sway angle were set to zero.

The desired CoM and body sway were initially set to zero, matching the zero value of the body sway angle when a subject was in the baseline pose. During the experiments the desired body sway angle was adapted to match the body sway angle of the steady pose that subjects maintained between perturbations, allowing for natural variation in forward lean [12]. The body sway velocity and CoM velocity were obtained by differentiating and low-pass filtering using a second order butterworth filter with a cut-off frequency of 10 Hz. The desired body sway velocity and whole body momentum were set to zero.

D. Protocol

We tested three control cases: PD_{com}, MBC and zero-impedance (ZI). Test-pilots received pushes with a push stick and had to recover from them without taking a step. Furthermore, they were instructed to return to the baseline pose after a push, to move their legs symmetrically and to keep the same stance width throughout the experiment. The push stick was equipped with a FUTEK LCM300 load cell (FUTEK Advanced Sensor Technology, Inc., Irvine, USA). The given push magnitudes, defined as the push force times the push duration, were about 80% and 60% of the maximum push magnitude defined in the tuning session, as shown in Table I. The experimenters that were giving the pushes were instructed to vary the push force, but keep the push duration constant. At all times, there was at least one spotter in front of the test-pilot to catch him in case of a near-fall. For each controller 40 pushes were given. Table I shows the trial order for each subject.

E. Data Collection and Analysis

The IMU data and joint encoder data were collected at the computer in the backpack at 1000 Hz. The push stick data were send to the analog input of an Input/Output-box (Ethercat slave) and also collected at 1000 Hz. For data analysis only responses were used to pushes that had a similar duration, that is, pushes with a duration deviating more than 0.1 s from the median push duration were dismissed. This was done for each test-pilot separately. Then the remaining pushes were sorted in groups of similar magnitudes. Though the attempted push magnitudes were about 80% and 60% of the maximum, these two groups could not be differentiated in the measured data. Therefore, for each test-pilot, pushes were sorted in two or three categories based on the push impulse distribution (Fig. 4).

The main outcome measures were the body sway amplitude and recovery time. The body sway amplitude was defined as the body sway angle in response to a push minus the mean body sway angle during the 1 second before the push. The recovery time after a push was based on the body sway velocity. The test-pilot was assumed to be recovered from a push when the absolute body sway velocity was smaller than 0.015 rad/s. The body sway amplitude and recovery time were computed for each response individually, before computing a mean over pushes of the same category.

III. RESULTS

We investigated the general behavior of the PD_{com} and MBC by analyzing their inputs and outputs. With both controllers, the body's CoM sways forward in response to a push, which corresponds to the decreasing body sway angle in Fig. 5A and the increasing CoM in Fig. 5B. As a result, both controllers generate a positive (plantar flexion) ankle torque (Fig. 5C,D). The magnitudes of the output torques of both controllers are not directly comparable, as they are dependent on the chosen controller gains. The generated knee torques were quite different for both controllers. The body sway controller produced a negative (extension) knee torque as the test-pilot kept his knee slightly bent (Fig. 5C). However, the MBC produced a positive (flexion) knee torque to prevent the CoM from moving forward and to reduce the momentum.

Considering the body sway amplitudes and recovery time, results were quite different for each test-pilot. For TP1 the sway amplitude clearly decreased when a balance controller was used. However, the recovery time was largest when using the MBC and shortest when using the PD_{com} (Fig. 6A). TP2 was not able to withstand any pushes with ZI, but could recover from the pushes when a controller was applied. The maximum body sway amplitude was almost the same for both balance controllers, but the recovery time was shorter for the MBC (Fig. 6B). Note that the recovery time was not computed over the mean body sway velocity, but for each response individually. For TP3 the body sway amplitude and recovery time were smallest when the PD_{com} was used (Fig. 6C). Although the recovery time using the MBC was only slightly different from the recovery time with ZI, the test-pilot clearly returned slower towards his baseline pose when no balance controller was applied. Fig. 6 only shows responses to pushes of category 2, but the results were consistent over all push categories.

IV. DISCUSSION

The goal of this study was to test whether the body sway controller and momentum-based controller could improve the standing balance recovery of paraplegics. Both controllers affected the body sway of the test-pilots in response to a perturbation. One of the test-pilots was not able to recover from pushes with zero-impedance, but could restore his balance when any of the controllers was implemented. For the other two test-pilots the body sway amplitude and recovery time could be reduced using the body sway controller. When the momentum-based controller was implemented, these test-pilots responded to a push faster, although the recovery time was not always shorter than with zero-impedance, indicating that it took the test-pilots more time to stand still.

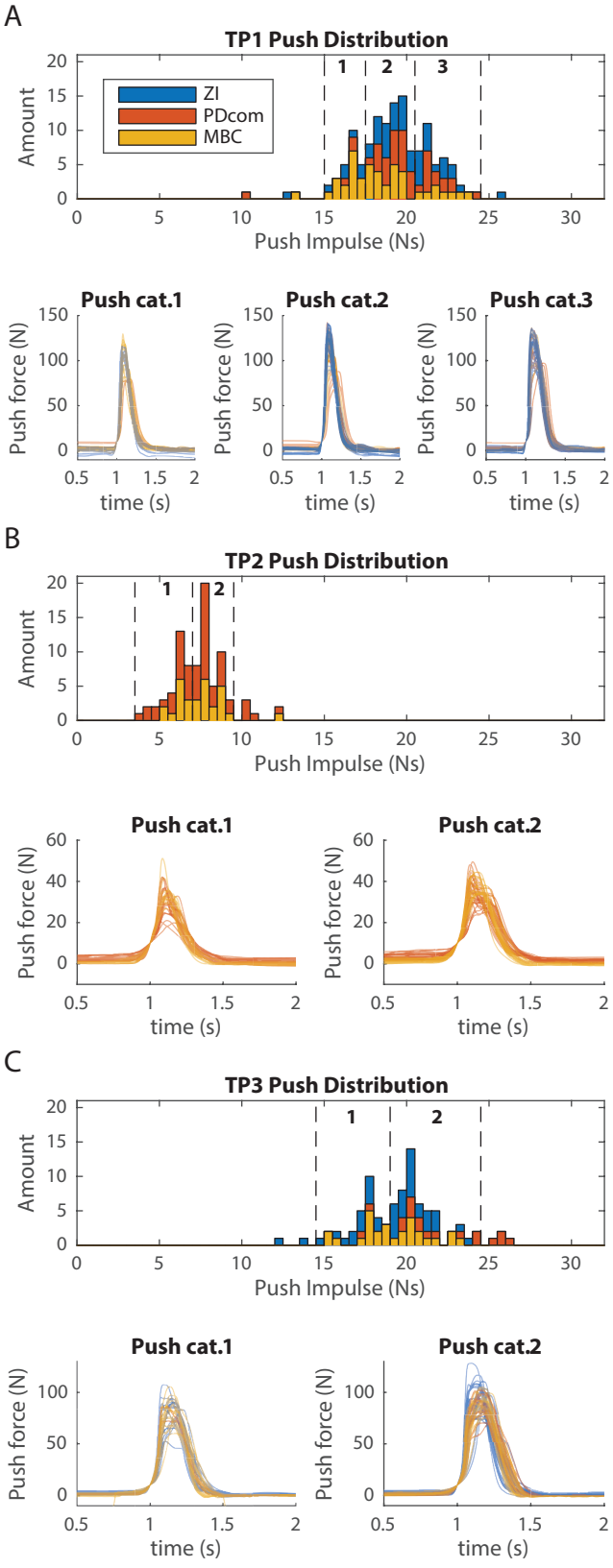

Fig. 4. Grouping of perturbations of similar magnitude. Underneath each histogram the individual push force trajectories are for each push category. The color of the trajectory corresponds to the controller.

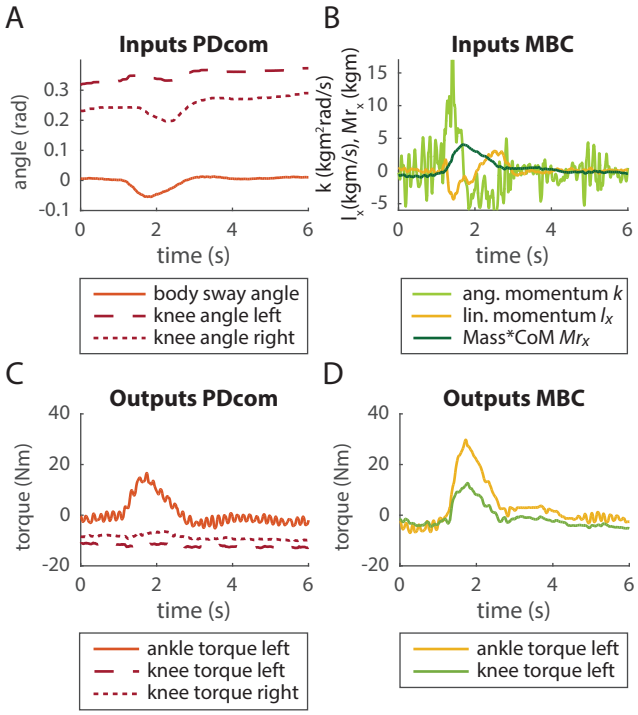

Fig. 5. Controller inputs and outputs. For the PD_{com} and MBC a typical response of TP3 to a category 2 push is shown. The body sway responses to these two pushes were similar. C: The PD_{com} generates a plantar flexion ankle torque and an extension knee torque. D: The MBC generates a plantar flexion ankle torque and a flexion knee torque.

In this study we focussed on standing balance in the sagittal plane. In this case the body sway controller performed better than the momentum-based controller. However, the body sway control strategy has the disadvantage that it cannot easily be extended to larger applications, such as exoskeletons with more degrees of freedom. The momentum-based control strategy on the other hand has already shown to perform well in complex balancing tasks of humanoids. Therefore it may still be worthy to further explore the possibilities of implementing momentum-based controllers on exoskeletons.

In the experiment we used a push stick to perturb the test-pilots and to measure the magnitude of the push. Advantages of the push stick are that it is easy to use and easy to carry along, but a disadvantage is the limited repeatability of the push magnitudes. Although we aimed to give pushes of certain predefined magnitudes, it turned out to be difficult to perturb consistently. For this experiment it was sufficient to group similar pushes afterwards, but when a higher accuracy is required an automated perturbation device [19] is more suitable.

A difficulty of this case study was that we were quite limited in the testing time, since the test-pilots were prone to fatiguing. As a consequence, the controller tuning for TP2 could not be done in one session (Table I). Furthermore we had to be quite pragmatic in our experimental protocols. For example, in one session we could not provide more pushes

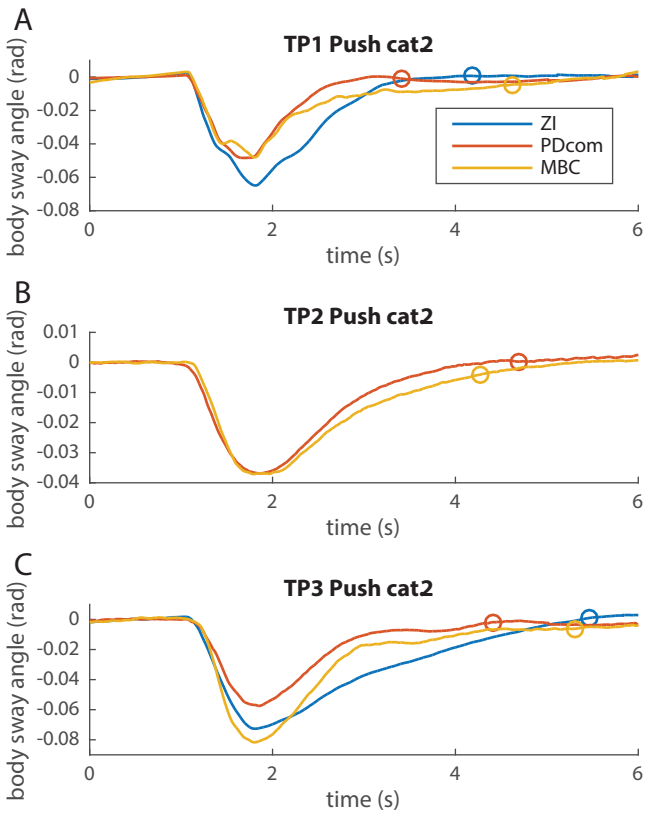

Fig. 6. Mean body sway amplitudes for each controller in response to cat. 2 pushes. The marker indicates the mean recovery time. Note that the recovery time was computed for each response individually before averaging.

or test various controller gains.

A major result of this study was that one of the test-pilots was able to recover from pushes when a balance controller was implemented on the exoskeleton, while this was not possible with zero-impedance. Still, the pushes he could handle were not quite as large as the pushes that were given to the other test-pilots. More extensive training with the device and the controllers might be necessary to further improve the balancing performance.

References

[1] J. Veneman, R. Kruidhof, E. Hekman, R. Ekkelenkamp, E. van Asseldonk, and H. van der Kooij, "Design and evaluation of the lopes exoskeleton robot for interactive gait rehabilitation," *IEEE Transactions on Neural Systems and Rehabilitation Engineering*, vol. 15, no. 3, pp. 379–386, 2007.

[2] S. Jezernik, G. Colombo, T. Keller, H. Frueh, and M. Morari, "Robotic orthosis lokomat: A rehabilitation and research tool," *Neuromodulation*, vol. 6, no. 2, pp. 108–115, 2003.

[3] E. Strickland, "Good-bye, wheelchair," *IEEE Spectrum*, vol. 49, no. 1, pp. 30–32, 2012.

[4] M. Bortole, A. Venkatakrishnan, F. Zhu, J. C. Moreno, G. E. Francisco, J. L. Pons, and J. L. Contreras-Vidal, "The h2 robotic exoskeleton for gait rehabilitation after stroke: Early findings from a clinical study," *Journal of NeuroEngineering and Rehabilitation*, vol. 12, no. 1, pp. 1–14, 2015.

[5] M. Aach, O. Cruciger, M. Sczesny-Kaiser, O. Hffken, R. C. Meindl, M. Tegenthoff, P. Schwenkreis, Y. Sankai, and T. A. Schildhauer, "Voluntary driven exoskeleton as a new tool for rehabilitation in chronic spinal cord injury: A pilot study," *The Spine Journal*, vol. 14, no. 12, pp. 2847 – 2853, 2014.

[6] S. Wang, L. Wang, C. Meijneke, E. van Asseldonk, T. Hoellinger, G. Cheron, Y. Ivanenko, V. La Scaleia, F. Sylos-Labini, M. Molinari, F. Tamburella, I. Pisotta, F. Thorsteinsson, M. Ilzkovitz, J. Gancet, Y. Nevatia, R. Hauffe, F. Zanow, and H. van der Kooij, "Design and control of the mindwalker exoskeleton," *IEEE Transactions on Neural Systems and Rehabilitation Engineering*, vol. 23, no. 2, pp. 277–286, March 2015.

[7] A. Esquenazi, M. Talaty, A. Packel, and M. Saulino, "The rewalk powered exoskeleton to restore ambulatory function to individuals with thoracic-level motor-complete spinal cord injury," *American Journal of Physical Medicine and Rehabilitation*, vol. 91, no. 11, pp. 911–921, 2012.

[8] R. J. Farris, H. A. Quintero, S. A. Murray, K. H. Ha, C. Hartigan, and M. Goldfarb, "A preliminary assessment of legged mobility provided by a lower limb exoskeleton for persons with paraplegia," *IEEE Transactions on Neural Systems and Rehabilitation Engineering*, vol. 22, no. 3, pp. 482–490, May 2014.

[9] Parker Haniffin Corp. (2016) Indego-powering people forward. [Online]. Available: http://www.indego.com/indego/en/home

[10] L. Wang, S. Wang, E. H. F. van Asseldonk, and H. van der Kooij, "Actively controlled lateral gait assistance in a lower limb exoskeleton," in *2013 IEEE/RSJ International Conference on Intelligent Robots and Systems*, Nov 2013, pp. 965–970.

[11] V. Rajasekaran, J. Aranda, A. Casals, and J. Pons, "An adaptive control strategy for postural stability using a wearable robot," *Robotics and Autonomous Systems*, vol. 73, pp. 16–23, 2015.

[12] A. R. Emmens, E. H. F. van Asseldonk, and H. van der Kooij, "Effects of a powered ankle-foot orthosis on perturbed standing balance," *Journal of NeuroEngineering and Rehabilitation*, vol. 15, no. 1, p. 50, Jun 2018.

[13] S. Kajita, F. Kanehiro, K. Kaneko, K. Fujiwara, K. Harada, K. Yokoi, and H. Hirukawa, "Resolved momentum control: humanoid motion planning based on the linear and angular momentum," in *Proceedings 2003 IEEE/RSJ International Conference on Intelligent Robots and Systems (IROS 2003) (Cat. No.03CH37453)*, vol. 2, Oct 2003, pp. 1644–1650 vol.2.

[14] S.-H. Lee and A. Goswami, "A momentum-based balance controller for humanoid robots on non-level and non-stationary ground," *Autonomous Robots*, vol. 33, no. 4, pp. 399–414, 2012.

[15] A. Herzog, L. Righetti, F. Grimminger, P. Pastor, and S. Schaal, "Balancing experiments on a torque-controlled humanoid with hierarchical inverse dynamics," in *Intelligent Robots and Systems (IROS 2014), 2014 IEEE/RSJ International Conference on*, Sept 2014, pp. 981–988.

[16] D. Orin and A. Goswami, "Centroidal momentum matrix of a humanoid robot: Structure and properties," in *Intelligent Robots and Systems, 2008. IROS 2008. IEEE/RSJ International Conference on*, Sept 2008, pp. 653–659.

[17] C. Meijneke, S. Wang, V. Sluiter, and H. van der Kooij, "Introducing a modular, personalized exoskeleton for ankle and knee support of individuals with a spinal cord injury," in *Wearable Robotics: Challenges and Trends*, J. González-Vargas, J. Ibáñez, J. L. Contreras-Vidal, H. van der Kooij, and J. L. Pons, Eds. Springer International Publishing, 2017, pp. 169–173.

[18] D. A. Winter, "Anthropometry," in *Biomechanics and Motor Control of Human Movement*, 4th ed. New York: John Wiley & Sons, Inc., 2009, pp. 82–106.

[19] M. Vlutters, E. H. F. van Asseldonk, and H. van der Kooij, "Center of mass velocity-based predictions in balance recovery following pelvis perturbations during human walking," *Journal of Experimental Biology*, vol. 219, no. 10, pp. 1514–1523, 2016.